Monthly Notices of the ROYAL ASTRONOMICAL SOCIETY

MNRAS **455,** 3480–3493 (2016) doi:10.1093/mnras/stv2512

A complete and explicit solution to the three-dimensional problem of two fixed centres

Francesco Biscani[1]★ and Dario Izzo[2]

[1]*Max Planck Institute for Astronomy, Königstuhl 17, D-69117 Heidelberg, Germany*
[2]*ESA – Advanced Concepts Team, European Space Research Technology Centre (ESTEC), Keplerlaan 1, Postbus 299, NL-2200 AG Noordwijk, the Netherlands*

Accepted 2015 October 26. Received 2015 October 23; in original form 2015 August 19

ABSTRACT

We present for the first time an explicit, complete and closed-form solution to the three-dimensional problem of two fixed centres, based on Weierstrass elliptic and related functions. With respect to previous treatments of the problem, our solution is exact, valid for all initial conditions and physical parameters of the system (including unbounded orbits and repulsive forces), and expressed via a unique set of formulae. Various properties of the three-dimensional problem of two fixed centres are investigated and analysed, with a particular emphasis on quasi-periodic and periodic orbits, regions of motion and equilibrium points.

Key words: gravitation – celestial mechanics.

1 INTRODUCTION

The problem of two fixed centres is the dynamical system consisting of two fixed bodies exerting inverse-square forces on a test particle. It is also known as Euler's three-body problem (E3BP), the Euler–Jacobi problem, and the two-centre Kepler problem, and it is the simplest three-body problem of physical interest. The solvability of the E3BP was first established by Euler in the 1760s, who demonstrated the existence of integrals of motion involving inverse square roots of quartic expressions. Later on, the E3BP attracted the attention of Legendre, Lagrange and Jacobi, who recognized that the solution of the E3BP can be expressed in terms of elliptic functions and integrals.

Throughout the twentieth century, mathematicians and astronomers frequently returned to the E3BP. Darboux (1901) showed how the E3BP can be generalized with the addition of complex masses at complex distances, while retaining separability in the elliptic coordinate system. Charlier (1902) used the E3BP as the starting point for a discussion of the restricted three-body problem in his treatise on celestial mechanics. Hiltebeitel (1911) introduced further generalizations of the E3BP involving linear and inverse-cube forces.

In the early days of quantum mechanics, the E3BP served as a model of the hydrogen molecule ion H_2^+ (Pauli 1922). The advent of the space age brought a renewed interest in the E3BP, after it was established that it could be used as an approximation of the potential of rotationally symmetric rigid bodies (Vinti 1959; Demin 1961; Aksenov, Grebenikov & Demin 1962; Deprit 1962; Aksenov, Grebenikov & Demin 1963; Alfriend et al. 1977). Even recently, the E3BP has been the subject of ongoing research, both in its classical formulation but also in connection with quantum mechanics and general relativity (Cordani 2003; Varvoglis, Vozikis & Wodnar 2004; Waalkens, Dullin & Richter 2004; Coelho & Herdeiro 2009). The work of Ó'Mathúna (2008) is particularly noteworthy, devoting four chapters to the E3BP.

From a purely mathematical point of view, the interest in the E3BP arises from the fact that it belongs to the very restrictive class of Liouville-integrable dynamical systems (Arnold 1989). From a physical and astronomical point of view, the E3BP is noteworthy for at least two reasons:

(i) as a (completely solvable) stepping-stone between the two-body problem and the three-body problem. In particular, the planar E3BP is analogous to a circular restricted three-body problem without centrifugal force;
(ii) as an approximation of the potential of a rotationally symmetric rigid body.

Despite more than two centuries of research, a full and explicit solution to the E3BP has so far proven elusive. As pointed out by Ó'Mathúna (2008), most authors explain that the solution involves elliptic functions and integrals, but they stop short of explicitly computing such solution or even sketching out how it is to be attained. This is particularly true for the three-dimensional E3BP, which is typically treated as an extension of the bidimensional case. Even in the very thorough exposition of Ó'Mathúna (2008), the solution of the three-dimensional E3BP is limited to the case of negative energy and it is not explicit in the third coordinate and in the time–angle relation.

The aim of this paper is to present for the first time a full explicit solution to the three-dimensional E3BP in terms of Weierstrass elliptic and related functions. Our solution is expressed via unique

★ E-mail: bluescarni@gmail.com

formulae valid for any set of physical parameters and initial conditions of the three-dimensional case. The use of the Weierstrassian formalism allows us to provide a compact formulation for the solution and to avoid the fragmentation usually associated with the use of Jacobi elliptic functions.

We need to point out that our focus is the three-dimensional case, and although the method presented here might also be suitable for the solution of the bidimensional case, we will not consider planar motion: our solution to the three-dimensional case stands alone and it is not formulated as a generalization of the bidimensional case. We also need to make clear that the main objective of this work is to detail the derivation of our solution and to present its general mathematical properties. The application to problems of astronomical and physical interest is left for subsequent publications.

The paper is structured as follows: in Section 2, we formulate the problem and we identify the integrals of motion in the Hamiltonian formalism; in Section 3, we solve the equations of motion and the time equation in elliptic–cylindrical coordinates; Section 4 is dedicated to the analysis of the solution, which focuses on periodic and quasi-periodic orbits, regions of motion, equilibrium points and displaced circular orbits; Section 5 is dedicated to the conclusions and to possible future extensions of the work presented here.

2 FORMULATION OF THE PROBLEM

The setup of the three-dimensional E3BP is sketched in Fig. 1. Without loss of generality, we can position the two centres on the positive and negative z-axis at a distance a from the origin of an inertial reference frame. This choice naturally allows us to take immediate advantage of the cylindrical symmetry of the problem, as it will be shown shortly. The Lagrangian of a test particle moving in the potential generated by the two fixed centres reads

$$\mathcal{L}(\boldsymbol{r};\dot{\boldsymbol{r}}) = \frac{\dot{\boldsymbol{r}}^2}{2} + \frac{\mu_1}{\sqrt{x^2+y^2+(z-a)^2}} + \frac{\mu_2}{\sqrt{x^2+y^2+(z+a)^2}}, \tag{1}$$

where $\boldsymbol{r} = (x, y, z)$ is the vector of Cartesian coordinates of the test particle, $\dot{\boldsymbol{r}}$ its time derivative, and $\mu_{1,2}$ represent the strength of the two centres of attraction. $\mu_{1,2}$ can either be positive or negative,

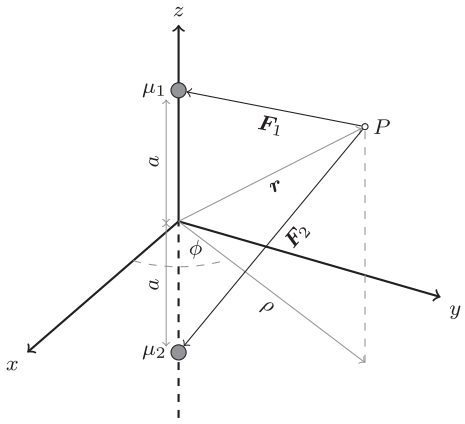

Figure 1. Setup of the three-dimensional E3BP. Two fixed centres μ_1 and μ_2 are located on the positive and negative z-axis at a distance a from the origin of an inertial frame of reference. μ_1 and μ_2 exert inverse-square forces $\boldsymbol{F}_1$ and $\boldsymbol{F}_2$ (attractive or repulsive) on a test particle P located at the position $\boldsymbol{r}$. The cylindrical radius ρ is the magnitude of the projection of $\boldsymbol{r}$ on the xy plane. ϕ is the azimuthal angle.

resulting, respectively, in attractive or repulsive forces on the test particle. In the gravitational E3BP, $\mu_{1,2}$ are gravitational parameters:

$$\mu_{1,2} = \mathcal{G}M_{1,2}, \tag{2}$$

where $M_{1,2}$ are the masses of the two centres and $\mathcal{G}$ is the gravitational constant. Although our solution is valid for both negative and positive $\mu_{1,2}$, in the analysis of the results we will focus on the gravitational E3BP, as it is arguably the most useful version of the E3BP in an astronomical context.

Following Waalkens et al. (2004), the first step of the separation of the problem is the introduction of cylindrical coordinates:

$$x = \rho\cos\phi, \quad \rho = \sqrt{x^2+y^2}, \tag{3}$$

$$y = \rho\sin\phi, \quad \phi = \arctan(y, x), \tag{4}$$

for the coordinates and

$$\dot{x} = \dot{\rho}\cos\phi - \rho\dot{\phi}\sin\phi, \quad \dot{\rho} = \frac{x\dot{x}+y\dot{y}}{\sqrt{x^2+y^2}}, \tag{5}$$

$$\dot{y} = \dot{\rho}\sin\phi + \rho\dot{\phi}\cos\phi, \quad \dot{\phi} = \frac{\dot{y}x-\dot{x}y}{x^2+y^2}, \tag{6}$$

for the velocities, where $\arctan(y, x)$ is the two-argument inverse tangent function. The Lagrangian in cylindrical coordinates reads

$$\mathcal{L}(\rho,\phi,z;\dot{\rho},\dot{\phi},\dot{z}) = \frac{\dot{\rho}^2+\rho^2\dot{\phi}^2+\dot{z}^2}{2} + \frac{\mu_1}{\sqrt{\rho^2+(z-a)^2}} + \frac{\mu_2}{\sqrt{\rho^2+(z+a)^2}}. \tag{7}$$

As a result of the rotational symmetry of the system, the ϕ coordinate is now cyclic and the Lagrangian is reduced to two degrees of freedom (in the variables ρ and z).

We now proceed to introduce elliptical coordinates on the (ρ, z) plane via the transformation

$$\rho = a\sqrt{(\xi^2-1)(1-\eta^2)}, \tag{8}$$

$$z = a\xi\eta, \tag{9}$$

its inverse

$$\xi = \frac{\sqrt{\rho^2+(z+a)^2}+\sqrt{\rho^2+(z-a)^2}}{2a}, \tag{10}$$

$$\eta = \frac{\sqrt{\rho^2+(z+a)^2}-\sqrt{\rho^2+(z-a)^2}}{2a}, \tag{11}$$

and the corresponding transformations for the velocities,

$$\dot{\rho} = a\frac{\dot{\xi}\xi(1-\eta^2)-\dot{\eta}\eta(\xi^2-1)}{\sqrt{(\xi^2-1)(1-\eta^2)}}, \tag{12}$$

$$\dot{z} = a(\dot{\xi}\eta+\xi\dot{\eta}), \tag{13}$$

and

$$\dot{\xi} = \frac{1}{2a}\left[\frac{\dot{\rho}\rho+\dot{z}(z+a)}{\sqrt{\rho^2+(z+a)^2}} + \frac{\dot{\rho}\rho+\dot{z}(z-a)}{\sqrt{\rho^2+(z-a)^2}}\right], \tag{14}$$

$$\dot{\eta} = \frac{1}{2a}\left[\frac{\dot{\rho}\rho+\dot{z}(z+a)}{\sqrt{\rho^2+(z+a)^2}} - \frac{\dot{\rho}\rho+\dot{z}(z-a)}{\sqrt{\rho^2+(z-a)^2}}\right]. \tag{15}$$

The right-hand side of equation (10) represents the sum of the distances of the point (ρ, z) from the two centres, normalized by $2a$. Similarly, the right-hand side of equation (11) represents the difference of the distances of the point (ρ, z) from the two centres, normalized by $2a$. It thus follows that the lines of constant ξ and η in the (ρ, z) plane are ellipses and branches of hyperbolae whose foci are coincident with the masses. The domain of ξ is $[1, \infty)$, the domain of η is $[-1, 1]$.

The Lagrangian in elliptic–cylindrical coordinates reads

$$\mathcal{L}\left(\xi, \eta, \phi; \dot{\xi}, \dot{\eta}, \dot{\phi}\right) = \frac{a^2}{2}\left[\frac{\dot{\xi}^2\xi^2\left(1-\eta^2\right)}{\xi^2-1} + \frac{\dot{\eta}^2\eta^2\left(\xi^2-1\right)}{1-\eta^2} + \dot{\phi}^2\left(\xi^2-1\right)\left(1-\eta^2\right) + \dot{\xi}^2\eta^2 + \xi^2\dot{\eta}^2\right] + \frac{\mu_1}{a\left(\xi-\eta\right)} + \frac{\mu_2}{a\left(\xi+\eta\right)}. \tag{16}$$

Switching now to the Hamiltonian formulation of the problem with a Legendre transformation, we introduce the generalized momenta via the relations

$$p_\xi = \frac{\partial\mathcal{L}}{\partial\dot{\xi}} = a^2\dot{\xi}\left(\frac{\xi^2-\eta^2}{\xi^2-1}\right), \tag{17}$$

$$p_\eta = \frac{\partial\mathcal{L}}{\partial\dot{\eta}} = a^2\dot{\eta}\left(\frac{\xi^2-\eta^2}{1-\eta^2}\right), \tag{18}$$

$$p_\phi = \frac{\partial\mathcal{L}}{\partial\dot{\phi}} = a^2\dot{\phi}\left(\xi^2-1\right)\left(1-\eta^2\right), \tag{19}$$

and the inverse

$$\dot{\xi} = \frac{p_\xi\left(\xi^2-1\right)}{a^2\left(\xi^2-\eta^2\right)}, \tag{20}$$

$$\dot{\eta} = \frac{p_\eta\left(1-\eta^2\right)}{a^2\left(\xi^2-\eta^2\right)}, \tag{21}$$

$$\dot{\phi} = \frac{p_\phi}{a^2\left(\xi^2-1\right)\left(1-\eta^2\right)}. \tag{22}$$

The Hamiltonian then reads

$$\mathcal{H}\left(p_\xi, p_\eta, p_\phi; \xi, \eta, \phi\right) = \frac{1}{2a^2\left(\xi^2-\eta^2\right)} \times \left[p_\xi^2\left(\xi^2-1\right) + p_\eta^2\left(1-\eta^2\right)\right] + \frac{p_\phi^2}{2a^2\left(\xi^2-1\right)\left(1-\eta^2\right)} - \frac{\mu_1}{a\left(\xi-\eta\right)} - \frac{\mu_2}{a\left(\xi+\eta\right)}. \tag{23}$$

p_ϕ is a constant of motion equal to the z component of the angular momentum per unit mass of the test particle. When p_ϕ is zero, the trajectory of the particle crosses the z-axis and it remains constrained to a plane (that is, the problem is reduced to the planar case). As explained earlier, we will not consider here this special case, and we always assume that p_ϕ is non-zero (or, equivalently, $\xi \neq 1$ and $\eta \neq \pm 1$).

We proceed now to the introduction of the new Hamiltonian $\mathcal{H}_\tau$, obtained through the following Poincaré time transformation (Siegel & Moser 1971; Carinena, Ibort & Lacomba 1988; Saha 2009):

$$\mathcal{H}_\tau = \left(\mathcal{H}-h\right)\left(\xi^2-\eta^2\right), \tag{24}$$

where h is the energy constant of the system (i.e. the numerical value of $\mathcal{H}$ after the substitution of the initial conditions into equation 23). The Hamiltonian $\mathcal{H}_\tau$ generates the equations of motion with respect to the new independent variable τ (often called a *fictitious* time), connected to the real time t through the differential relation

$$\mathrm{d}t = \left(\xi^2-\eta^2\right)\mathrm{d}\tau. \tag{25}$$

The Poincaré time transform can be seen as the Hamiltonian analogue of a Sundman transformation (Sundman 1912): it regularizes the problem by slowing time down when the particle is close to either fixed centre (note how in correspondence of the two centres $\xi^2 - \eta^2$ is zero).

The equations of motion in fictitious time read

$$\frac{\mathrm{d}\xi}{\mathrm{d}\tau} = \frac{\partial\mathcal{H}_\tau}{\partial p_\xi}, \quad \frac{\mathrm{d}p_\xi}{\mathrm{d}\tau} = -\frac{\partial\mathcal{H}_\tau}{\partial\xi}, \tag{26}$$

$$\frac{\mathrm{d}\eta}{\mathrm{d}\tau} = \frac{\partial\mathcal{H}_\tau}{\partial p_\eta}, \quad \frac{\mathrm{d}p_\eta}{\mathrm{d}\tau} = -\frac{\partial\mathcal{H}_\tau}{\partial\eta}, \tag{27}$$

$$\frac{\mathrm{d}\phi}{\mathrm{d}\tau} = \frac{\partial\mathcal{H}_\tau}{\partial p_\phi}, \quad \frac{\mathrm{d}p_\phi}{\mathrm{d}\tau} = -\frac{\partial\mathcal{H}_\tau}{\partial\phi}, \tag{28}$$

while the complete expression for $\mathcal{H}_\tau$ is

$$\mathcal{H}_\tau\left(p_\xi, p_\eta, p_\phi; \xi, \eta, \phi\right) = -\xi^2 h - \frac{\xi}{a}\left(\mu_1+\mu_2\right) + \frac{p_\phi^2}{2a^2\left(\xi^2-1\right)} + \frac{p_\xi^2}{2a^2}\left(\xi^2-1\right) + \eta^2 h - \frac{\eta}{a}\left(\mu_1-\mu_2\right) + \frac{p_\phi^2}{2a^2\left(1-\eta^2\right)} + \frac{p_\eta^2}{2a^2}\left(1-\eta^2\right). \tag{29}$$

The Hamiltonian $\mathcal{H}_\tau$ has thus been separated into the two constants of motion

$$h_\xi = -\xi^2 h - \frac{\xi}{a}\left(\mu_1+\mu_2\right) + \frac{p_\phi^2}{2a^2\left(\xi^2-1\right)} + \frac{p_\xi^2}{2a^2}\left(\xi^2-1\right), \tag{30}$$

$$h_\eta = \eta^2 h - \frac{\eta}{a}\left(\mu_1-\mu_2\right) + \frac{p_\phi^2}{2a^2\left(1-\eta^2\right)} + \frac{p_\eta^2}{2a^2}\left(1-\eta^2\right). \tag{31}$$

We can now move on to the solution of the equations of motion.

3 INTEGRATION OF THE EQUATIONS OF MOTION

We proceed now to the explicit integration of the equations of motion (26)–(28) and of the time equation (25). We detail initially the solution for the ξ coordinate; the solution for the η coordinate if formally identical, while the solutions for the ϕ coordinate and for the time equation require a different procedure. The solutions for the momenta p_ξ and p_η will be easily computed via the solutions for ξ and η. In this section, we will focus on the mathematical details of the solution. Section 4 will be dedicated to the analysis of our results.

3.1 Solution for ξ

The equation of motion for ξ, equation (26), reads

$$\frac{\mathrm{d}\xi}{\mathrm{d}\tau} = \frac{\xi^2 p_\xi}{a^2} - \frac{p_\xi}{a^2}. \tag{32}$$

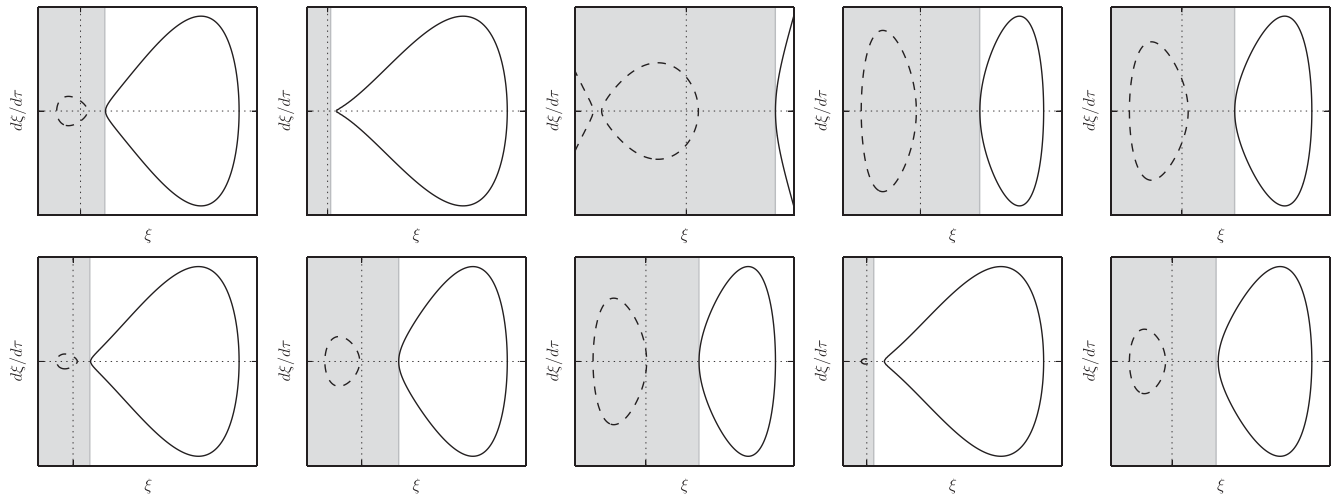

Figure 2. Phase portraits for the ξ variable in 10 randomly generated cases. The shaded region corresponding to $\xi < 1$ is the domain in which the ξ variable does not represent any real physical coordinate. The trajectories in the $(\xi, \mathrm{d}\xi/\mathrm{d}\tau)$ plane are elliptic curves. All the portraits refer to bounded trajectories, apart from the third panel in the first row.

We can use the constant of motion h_ξ to express p_ξ as a function of ξ, via the inversion of equation (30):

$$p_\xi = \pm \frac{1}{\xi^2 - 1} \sqrt{f_\xi(\xi)}, \tag{33}$$

where

$$\begin{aligned} f_\xi(\xi) = {} & 2\xi^4 a^2 h + \xi^3 (2\mu_1 a + 2\mu_2 a) \\ & + \xi^2 \left(-2a^2 h + 2a^2 h_\xi\right) + \xi(-2\mu_1 a - 2\mu_2 a) \\ & - 2a^2 h_\xi - p_\phi^2 \end{aligned} \tag{34}$$

is a polynomial of degree 4 in ξ. The equation of motion for ξ then reads

$$\frac{\mathrm{d}\xi}{\mathrm{d}\tau} = \pm \frac{\sqrt{f_\xi(\xi)}}{a^2}. \tag{35}$$

Before proceeding to the integration and inversion of this equation, we need to highlight a useful property of $f_\xi(\xi)$. It can be checked by direct substitution that

$$f_\xi(1) = -p_\phi^2 < 0, \tag{36}$$

that is, the value of the polynomial is always negative for $\xi = 1$. On the other hand, for any choice of initial conditions, $f_\xi(\xi)$ must assume positive values in a subrange of $\xi > 1$, otherwise the radicand in equation (35) would be negative. Consequently, the polynomial $f_\xi(\xi)$ must have at least one real root in the range $(1, +\infty)$ (i.e. in the domain of interest for the variable ξ). Fig. 2 visualizes the phase portraits for ξ in a few randomly selected cases. It should be noted how a necessary condition for unbounded motion is a positive energy constant h: according to equations (34) and (35), if h is negative the radicand on the right-hand side of equation (35) assumes negative values for $\xi \to \infty$. Thus, for negative h the phase portrait for the ξ variable must be a closed curve.

The integration by quadrature of equation (35) reads

$$\int_{\xi_0}^{\xi} \frac{\mathrm{d}s}{\sqrt{f_\xi(s)}} = \pm \frac{1}{a^2} \int_0^\tau \mathrm{d}s, \tag{37}$$

where s is a dummy integration variable, ξ_0 is an arbitrary initial value for ξ and, without loss of generality, we have set the initial fictitious time to 0. The $\pm$ sign in front of the integral on the right-hand side can be chosen as the sign of the initial value of $\mathrm{d}\xi/\mathrm{d}\tau$. With this convention, the right-hand side of equation (37) represents the time needed by the system to evolve from ξ_0 to ξ along a trajectory in which the sign of $\mathrm{d}\xi/\mathrm{d}\tau$ is constant.

The left-hand side of equation (37) is an elliptic integral which can be inverted to yield $\xi(\tau)$ using a formula by Weierstrass, reported in Whittaker & Watson (1927, section 20.6). The general formula is rather complicated, but it can be simplified considerably by choosing as the initial value for the integration a root ξ_r of the polynomial $f_\xi(\xi)$. With such a choice, equation (37) reads

$$\int_{\xi_r}^{\xi} \frac{\mathrm{d}s}{\sqrt{f_\xi(s)}} = \pm \frac{1}{a^2} \int_{\tau_\xi}^{\tau} \mathrm{d}s, \tag{38}$$

where now τ_ξ is the fictitious *time of root passage* for ξ. In analogy with the Kepler problem, when ξ_r is the smallest reachable root in the domain of interest τ_ξ can be considered as a kind of fictitious 'time of pericentre passage' for the ξ variable. τ_ξ can be computed by solving the elliptic integral

$$\tau_\xi = \pm a^2 \int_{\xi_0}^{\xi_r} \frac{\mathrm{d}s}{\sqrt{f_\xi(s)}}. \tag{39}$$

As we have mentioned above, the existence of at least one root ξ_r in the domain of interest for ξ is guaranteed by the properties of the coefficients of $f_\xi(\xi)$. ξ_r can be computed either numerically or algebraically (via the quartic formula).

Equation (38) can now be integrated and inverted to yield

$$\xi(\tau) = \xi_r + \frac{1}{4} \frac{f_\xi'(\xi_r)}{\wp_\xi\left(\frac{\tau - \tau_\xi}{a^2}\right) - \frac{1}{24} f_\xi''(\xi_r)}. \tag{40}$$

In this formula, the derivatives of $f_\xi(\xi)$ are to be taken with respect to ξ, and $\wp_\xi$ is a Weierstrass elliptic function defined in terms of the two *invariants*

$$\begin{aligned} g_2 = {} & \mu_1^2 a^2 + 2\mu_1\mu_2 a^2 + \mu_2^2 a^2 + \frac{a^4 h^2}{3} - \frac{14\,h}{3} a^4 h_\xi \\ & + \frac{a^4 h_\xi^2}{3} - 2a^2 h p_\phi^2, \end{aligned} \tag{41}$$

$$
\begin{aligned}
g_3 = &-\frac{\mu_1^2 h}{3}a^4 + \frac{\mu_1^2 h_\xi}{3}a^4 + \frac{\mu_1^2 p_\phi^2}{4}a^2 \\
&- \frac{2\mu_1}{3}\mu_2 a^4 h + \frac{2\mu_1}{3}\mu_2 a^4 h_\xi + \frac{\mu_1\mu_2}{2}a^2 p_\phi^2 \\
&- \frac{\mu_2^2 h}{3}a^4 + \frac{\mu_2^2 h_\xi}{3}a^4 + \frac{\mu_2^2 p_\phi^2}{4}a^2 \\
&+ \frac{a^6 h^3}{27} + \frac{11 h_\xi}{9}a^6 h^2 - \frac{11\,h}{9}a^6 h_\xi^2 - \frac{a^6 h_\xi^3}{27} \\
&+ \frac{2\,h^2}{3}a^4 p_\phi^2 - \frac{2\,h}{3}a^4 h_\xi p_\phi^2,
\end{aligned} \tag{42}
$$

computed from the coefficients of the polynomial $f_\xi(\xi)$ following Whittaker & Watson (1927, section 20.6). Without giving a full account of the theory of the Weierstrassian functions (for which we refer to standard textbooks such as Whittaker & Watson 1927, Abramowitz & Stegun 1964 and Akhiezer 1990), we will recall here briefly a few fundamental notions about the $\wp$ function. As commonly done, in the following we will suppress the verbose notation $\wp_\xi(\tau; g_2, g_3)$ in favour of just $\wp_\xi(\tau)$, with the understanding that $\wp_\xi$ refers to a Weierstrass function defined in terms of the invariants (41) and (42).

The elliptic function $\wp(z; g_2, g_3)$ is a doubly periodic complex-valued function of a complex variable z defined in terms of the two invariants g_2 and g_3. The complex primitive half-periods of $\wp$ can be related to the invariants via formulae involving elliptic integrals and the roots e_1, e_2 and e_3 of the Weierstrass cubic

$$
4t^3 - g_2 t - g_3 = 0 \tag{43}
$$

(e.g. see Abramowitz & Stegun 1964, section 18.9). The sign of the *modular discriminant*

$$
\Delta = g_2^3 - 27 g_3^2 \tag{44}
$$

determines the nature of the roots e_1, e_2 and e_3. In this specific case, the invariants are by definition real, τ is also real, and $\wp_\xi(\tau)$ can thus be regarded as a real-valued singly periodic function on the real axis (see Abramowitz & Stegun 1964, chapter 18). We refer to the real half-period of $\wp_\xi$ as ω_ξ. It should be noted that, according to equation (39), if the real period of $\wp_\xi$ is $2\omega_\xi$, then the period of $\xi(\tau)$ is $2a^2\omega_\xi$.

$\wp$ is an even function, and it has second-order poles at each point of the period lattice. That is, $\wp_\xi$ satisfies the following properties (where $k \in \mathbb{Z}$):

$$
\wp_\xi(\tau) = \wp_\xi\left(\tau + 2k\omega_\xi\right), \tag{45}
$$

$$
\wp_\xi(\tau) = \wp_\xi(-\tau), \tag{46}
$$

$$
\lim_{\tau \to 2k\omega_\xi} \wp_\xi(\tau) = +\infty, \tag{47}
$$

and in proximity of $\tau = 2k\omega_\xi$ the function $\wp_\xi(\tau)$ behaves, on the real axis, like $1/\tau^2$ in proximity of $\tau = 0$. Fig. 3 illustrates graphically the behaviour of the Weierstrass elliptic function on the real axis.

We can also use the inverse Weierstrass elliptic function $\wp^{-1}$ to express the time of root passage via the inversion of equation (40) after setting $\tau = 0$:

$$
\tau_\xi = a^2 \wp_\xi^{-1}\left[\frac{1}{24}f_\xi''(\xi_r) + \frac{f_\xi'(\xi_r)}{4(\xi_0 - \xi_r)}\right]. \tag{48}
$$

This is an alternative (but equivalent) formulation of the elliptic integral (39). It must be noted that the function $\wp^{-1}$ has two solutions

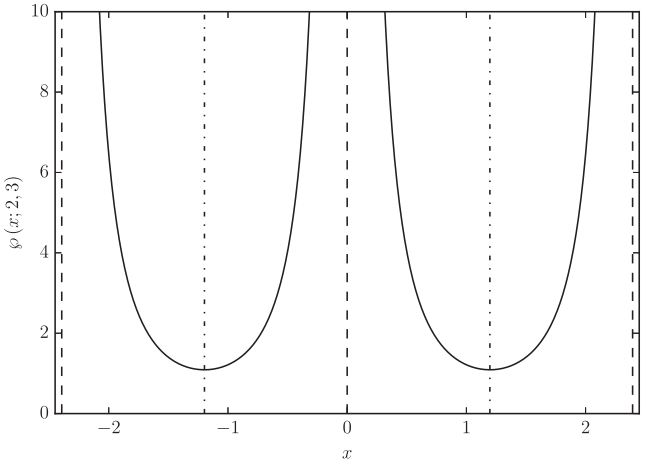

Figure 3. Plot of $\wp(2, 3; z)$ on the real axis over two real periods (solid line). In this specific case, the real period 2ω is approximately 2.39. The vertical dashed lines represent asymptotes, close to which $\wp$ behaves like $1/z^2$ close to zero. The vertical dash–dotted lines in correspondence of the real half-period ω cross $\wp$ at its absolute minimum value, and they are axes of symmetry for $\wp$ within the real period.

within the fundamental parallelogram of $\wp$, and thus two possible values for τ_ξ exist. This ambiguity physically translates to the fact that each value assumed by the ξ coordinate is visited twice along a trajectory, once with a positive value for $\mathrm{d}\xi/\mathrm{d}\tau$ and once with a negative value.[1] The correct choice for τ_ξ is the value which, when plugged into equation (75) (which describes the evolution of p_ξ in fictitious time), returns the initial value of p_ξ.

3.2 Solution for η

The equation of motion for η, equation (27), reads

$$
\frac{\mathrm{d}\eta}{\mathrm{d}\tau} = -\frac{\eta^2 p_\eta}{a^2} + \frac{p_\eta}{a^2}. \tag{49}
$$

Following the same procedure adopted for ξ, we can express p_η by inverting equation (31), and rewrite the equation of motion as

$$
\frac{\mathrm{d}\eta}{\mathrm{d}\tau} = \pm\frac{\sqrt{f_\eta(\eta)}}{a^2}, \tag{50}
$$

where $f_\eta(\eta)$ is a polynomial of degree 4 in η:

$$
\begin{aligned}
f_\eta(\eta) = &\, 2\eta^4 a^2 h + \eta^3(-2\mu_1 a + 2\mu_2 a) \\
&+ \eta^2\left(-2a^2 h - 2a^2 h_\eta\right) + \eta(2\mu_1 a - 2\mu_2 a) \\
&+ 2a^2 h_\eta - p_\phi^2.
\end{aligned} \tag{51}
$$

It is easy to verify by direct substitution that

$$
f_\eta(\pm 1) = -p_\phi^2 < 0, \tag{52}
$$

which implies that in the domain of interest, $\eta \in (-1, 1)$, the polynomial $f_\eta(\eta)$ must have real roots. Fig. 4 visualizes the phase portraits for η in a few randomly selected cases.

We can then adopt also for η the simplified inversion method from Whittaker & Watson (1927, section 20.6), and write the solution of

[1] Another manifestation of this ambiguity is the symmetry with respect to the horizontal axis of the phase portraits – see the examples in Fig. 2.

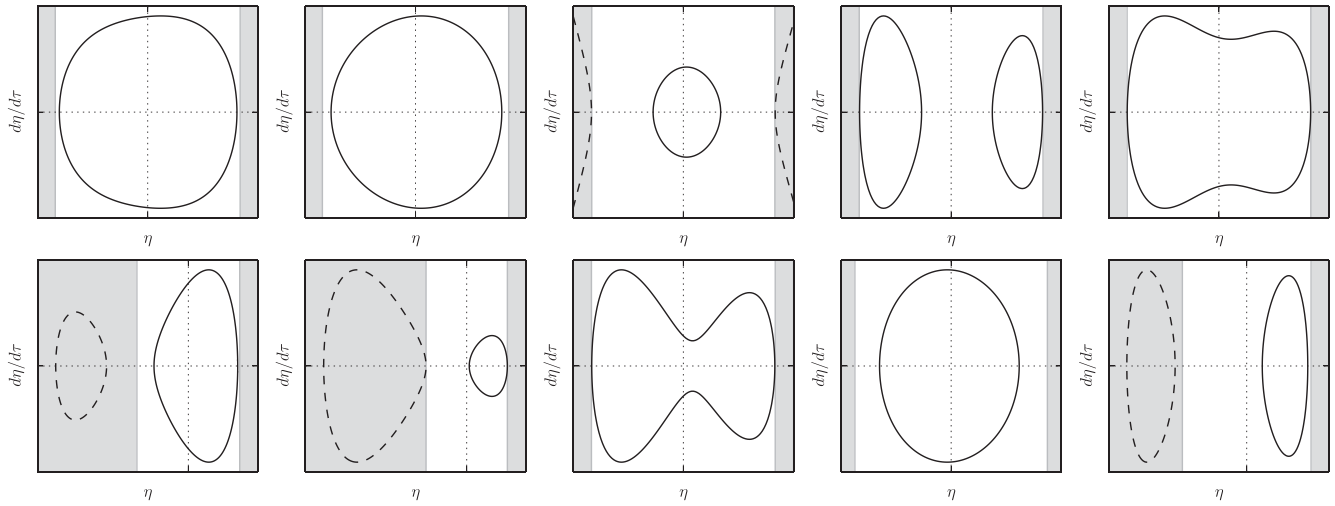

Figure 4. Phase portraits for the η variable in 10 randomly generated cases. The shaded regions corresponding to $\eta < -1$ and $\eta > 1$ are the domains in which the η variable does not represent any real physical coordinate. The trajectories in the $(\eta, \mathrm{d}\eta/\mathrm{d}\tau)$ plane are elliptic curves.

equation (50) as

$$\eta(\tau) = \eta_r + \frac{1}{4}\frac{f'_\eta(\eta_r)}{\wp_\eta\left(\frac{\tau-\tau_\eta}{a^2}\right) - \frac{1}{24}f''_\eta(\eta_r)}. \tag{53}$$

Analogously to ξ_r, η_r is a root of the polynomial $f_\eta(\eta)$ and τ_η is the fictitious time of root passage for the variable η. The Weierstrassian function $\wp_\eta$ is defined in terms of the two invariants

$$\begin{aligned} g_2 = {} & \mu_1^2 a^2 - 2\mu_1\mu_2 a^2 + \mu_2^2 a^2 + \frac{a^4 h^2}{3} + \frac{14\,h}{3}a^4 h_\eta \\ & + \frac{a^4 h_\eta^2}{3} - 2a^2 h p_\phi^2, \end{aligned} \tag{54}$$

$$\begin{aligned} g_3 = {} & -\frac{\mu_1^2 h}{3}a^4 - \frac{\mu_1^2 h_\eta}{3}a^4 + \frac{\mu_1^2 p_\phi^2}{4}a^2 \\ & + \frac{2\mu_1}{3}\mu_2 a^4 h + \frac{2\mu_1}{3}\mu_2 a^4 h_\eta - \frac{\mu_1\mu_2}{2}a^2 p_\phi^2 \\ & - \frac{\mu_2^2 h}{3}a^4 - \frac{\mu_2^2 h_\eta}{3}a^4 + \frac{\mu_2^2 p_\phi^2}{4}a^2 \\ & + \frac{a^6 h^3}{27} - \frac{11 h_\eta}{9}a^6 h^2 - \frac{11\,h}{9}a^6 h_\eta^2 + \frac{a^6 h_\eta^3}{27} \\ & + \frac{2\,h^2}{3}a^4 p_\phi^2 + \frac{2\,h}{3}a^4 h_\eta p_\phi^2, \end{aligned} \tag{55}$$

and τ_η can be calculated as

$$\tau_\eta = a^2 \wp_\eta^{-1}\left[\frac{1}{24}f''_\eta(\eta_r) + \frac{f'_\eta(\eta_r)}{4(\eta_0 - \eta_r)}\right]. \tag{56}$$

In analogy with the notation adopted for ξ, we refer to the real period of $\wp_\eta$ as $2\omega_\eta$. The period of $\eta(\tau)$ is $2a^2\omega_\eta$.

3.3 Solution for ϕ and for the time equation

The equation of motion for ϕ, equation (28), and the time equation, equation (25), read

$$\frac{\mathrm{d}\phi}{\mathrm{d}\tau} = \frac{p_\phi}{a^2}\left[\frac{1}{\xi^2(\tau) - 1} + \frac{1}{1 - \eta^2(\tau)}\right], \tag{57}$$

$$\frac{\mathrm{d}t}{\mathrm{d}\tau} = \xi^2(\tau) - \eta^2(\tau). \tag{58}$$

The solution of these two equations involves the integration by quadrature of a rational function of Weierstrass elliptic functions. In order reduce visual clutter, we introduce the notation

$$A_\xi = f'_\xi(\xi_r), \quad A_\eta = f'_\eta(\eta_r), \tag{59}$$

$$B_\xi = \frac{1}{24}f''_\xi(\xi_r), \quad B_\eta = \frac{1}{24}f''_\eta(\eta_r). \tag{60}$$

A_ξ, B_ξ, A_η and B_η are all constants of motion depending on the physical parameters of the system and on the initial conditions.

The general theory of the integration of rational functions of Weierstrass elliptic functions is given, e.g. in Halphen (1886, Chapter VII) and Greenhill (1959, Chapter VII). Here, it will be enough to first perform a fraction decomposition with respect to $\wp$, and then to integrate the decomposed fractions using the formulae from Tannery & Molk (1893, Chapter CXII). After the substitution of equations (40) and (53) into equation (57), the decomposition for $\mathrm{d}\phi/\mathrm{d}\tau$ is

$$\begin{aligned} \frac{\mathrm{d}\phi}{\mathrm{d}\tau} = {} & \frac{p_\phi A_\xi}{8a^2(\xi_r+1)^2\left[\wp_\xi\left(\frac{\tau-\tau_\xi}{a^2}\right) + \frac{A_\xi - 4B_\xi\xi_r - 4B_\xi}{4(\xi_r+1)}\right]} \\ & - \frac{p_\phi A_\xi}{8a^2(\xi_r-1)^2\left[\wp_\xi\left(\frac{\tau-\tau_\xi}{a^2}\right) + \frac{A_\xi - 4B_\xi\xi_r + 4B_\xi}{4(\xi_r-1)}\right]} \\ & - \frac{p_\phi A_\eta}{8a^2(\eta_r+1)^2\left[\wp_\eta\left(\frac{\tau-\tau_\eta}{a^2}\right) + \frac{A_\eta - 4B_\eta\eta_r - 4B_\eta}{4(\eta_r+1)}\right]} \\ & + \frac{p_\phi A_\eta}{8a^2(\eta_r-1)^2\left[\wp_\eta\left(\frac{\tau-\tau_\eta}{a^2}\right) + \frac{A_\eta - 4B_\eta\eta_r + 4B_\eta}{4(\eta_r-1)}\right]} \\ & + \frac{p_\phi}{a^2\left(\xi_r^2 - 1\right)} - \frac{p_\phi}{a^2\left(\eta_r^2 - 1\right)}. \end{aligned} \tag{61}$$

The decomposition for $\mathrm{d}t/\mathrm{d}\tau$ reads

$$\begin{aligned} \frac{\mathrm{d}t}{\mathrm{d}\tau} = {} & \frac{A_\xi^2}{16\left[\wp_\xi\left(\frac{\tau-\tau_\xi}{a^2}\right) - B_\xi\right]^2} + \frac{A_\xi\xi_r}{2\left[\wp_\xi\left(\frac{\tau-\tau_\xi}{a^2}\right) - B_\xi\right]} + \xi_r^2 \\ & - \frac{A_\eta^2}{16\left[\wp_\eta\left(\frac{\tau-\tau_\eta}{a^2}\right) - B_\eta\right]^2} - \frac{A_\eta\eta_r}{2\left[\wp_\eta\left(\frac{\tau-\tau_\eta}{a^2}\right) - B_\eta\right]} - \eta_r^2. \end{aligned} \tag{62}$$

In order to integrate equations (61) and (62), we employ two formulae from Tannery & Molk (1893, Chapter CXII) (see also Gradshteĭn & Ryzhik 2007, section 5.141):

$$\int \frac{\mathrm{d}u}{\wp(u)-\wp(v)} = \frac{1}{\wp'(v)}\left[\ln\frac{\sigma(u-v)}{\sigma(u+v)} + 2u\zeta(v)\right], \tag{63}$$

$$\int \frac{\mathrm{d}u}{\left[\wp(u)-\wp(v)\right]^2} = \frac{1}{\wp'^2(v)}\left[-\zeta(u-v)-\zeta(u+v) - 2u\wp(v)-\wp''(v)\int\frac{\mathrm{d}u}{\wp(u)-\wp(v)}\right]. \tag{64}$$

It can easily be recognized how the terms in equations (61) and (62) are in the form of the integrands on the left-hand sides of equations (63) and (64) (modulo additive and multiplicative constants).[2,3]

Following Tannery & Molk (1893, Chapter CXII), we introduce the shorthand notation for the two integrals (63) and (64)

$$\mathcal{J}_1(u,v) = \int \frac{\mathrm{d}u}{\wp(u)-\wp(v)}, \tag{65}$$

$$\mathcal{J}_2(u,v) = \int \frac{\mathrm{d}u}{\left[\wp(u)-\wp(v)\right]^2} \tag{66}$$

(with the understanding that we will add a ξ or η subscript depending on the subscript of the Weierstrassian functions appearing in the integrals). With this convention, we can integrate equation (61) and obtain

$$\begin{aligned}\phi(\tau) = \phi_0 &+ \frac{p_\phi A_\xi}{8(\xi_r+1)^2}\left[\mathcal{J}_{\xi,1}\left(\frac{\tau-\tau_\xi}{a^2}, v_{\xi,1}\right) - \mathcal{J}_{\xi,1}\left(-\frac{\tau_\xi}{a^2}, v_{\xi,1}\right)\right]\\ &- \frac{p_\phi A_\xi}{8(\xi_r-1)^2}\left[\mathcal{J}_{\xi,1}\left(\frac{\tau-\tau_\xi}{a^2}, v_{\xi,2}\right) - \mathcal{J}_{\xi,1}\left(-\frac{\tau_\xi}{a^2}, v_{\xi,2}\right)\right]\\ &- \frac{p_\phi A_\eta}{8(\eta_r+1)^2}\left[\mathcal{J}_{\eta,1}\left(\frac{\tau-\tau_\eta}{a^2}, v_{\eta,1}\right) - \mathcal{J}_{\eta,1}\left(-\frac{\tau_\eta}{a^2}, v_{\eta,1}\right)\right]\\ &+ \frac{p_\phi A_\eta}{8(\eta_r-1)^2}\left[\mathcal{J}_{\eta,1}\left(\frac{\tau-\tau_\eta}{a^2}, v_{\eta,2}\right) - \mathcal{J}_{\eta,1}\left(-\frac{\tau_\eta}{a^2}, v_{\eta,2}\right)\right]\\ &+ \frac{p_\phi\tau}{a^2\left(\xi_r^2-1\right)} - \frac{p_\phi\tau}{a^2\left(\eta_r^2-1\right)},\end{aligned} \tag{67}$$

where we have introduced the constants

$$v_{\xi,1} = \wp^{-1}\left[-\frac{A_\xi - 4B_\xi\xi_r - 4B_\xi}{4(\xi_r+1)}\right], \tag{68}$$

$$v_{\xi,2} = \wp^{-1}\left[-\frac{A_\xi - 4B_\xi\xi_r + 4B_\xi}{4(\xi_r-1)}\right], \tag{69}$$

$$v_{\eta,1} = \wp^{-1}\left[-\frac{A_\eta - 4B_\eta\eta_r - 4B_\eta}{4(\eta_r+1)}\right], \tag{70}$$

$$v_{\eta,2} = \wp^{-1}\left[-\frac{A_\eta - 4B_\eta\eta_r + 4B_\eta}{4(\eta_r-1)}\right] \tag{71}$$

in order to simplify the notation. Analogously, the integration of equation (62) yields

$$\begin{aligned}t(\tau) = &\frac{a^2A_\xi^2}{16}\left[\mathcal{J}_{\xi,2}\left(\frac{\tau-\tau_\xi}{a^2}, b_\xi\right) - \mathcal{J}_{\xi,2}\left(-\frac{\tau_\xi}{a^2}, b_\xi\right)\right]\\ &+ \frac{a^2A_\xi\xi_r}{2}\left[\mathcal{J}_{\xi,1}\left(\frac{\tau-\tau_\xi}{a^2}, b_\xi\right) - \mathcal{J}_{\xi,1}\left(-\frac{\tau_\xi}{a^2}, b_\xi\right)\right]\\ &- \frac{a^2A_\eta^2}{16}\left[\mathcal{J}_{\eta,2}\left(\frac{\tau-\tau_\eta}{a^2}, b_\eta\right) - \mathcal{J}_{\eta,2}\left(-\frac{\tau_\eta}{a^2}, b_\eta\right)\right]\\ &- \frac{a^2A_\eta\eta_r}{2}\left[\mathcal{J}_{\eta,1}\left(\frac{\tau-\tau_\eta}{a^2}, b_\eta\right) - \mathcal{J}_{\eta,1}\left(-\frac{\tau_\eta}{a^2}, b_\eta\right)\right]\\ &+ \left(\xi_r^2-\eta_r^2\right)\tau,\end{aligned} \tag{72}$$

where we have introduced the constants

$$b_\xi = \wp_\xi^{-1}\left(B_\xi\right), \tag{73}$$

$$b_\eta = \wp_\eta^{-1}\left(B_\eta\right) \tag{74}$$

again in order to simplify the notation.

3.4 Solution for p_ξ and p_η

The explicit solution in fictitious time for p_ξ and p_η can be computed by inverting equations (32) and (49) to yield

$$p_\xi(\tau) = \frac{a^2}{\xi^2(\tau)-1}\frac{\mathrm{d}\xi(\tau)}{\mathrm{d}\tau}, \tag{75}$$

$$p_\eta(\tau) = \frac{a^2}{1-\eta^2(\tau)}\frac{\mathrm{d}\eta(\tau)}{\mathrm{d}\tau}. \tag{76}$$

The derivatives of $\xi(\tau)$ and $\eta(\tau)$ can be computed from the solutions (40) and (53):

$$\frac{\mathrm{d}\xi(\tau)}{\mathrm{d}\tau} = -\frac{A_\xi\wp_\xi'\left(\frac{\tau-\tau_\xi}{a^2}\right)}{4a^2\left[\wp_\xi\left(\frac{\tau-\tau_\xi}{a^2}\right) - B_\xi\right]^2}, \tag{77}$$

$$\frac{\mathrm{d}\eta(\tau)}{\mathrm{d}\tau} = -\frac{A_\eta\wp_\eta'\left(\frac{\tau-\tau_\eta}{a^2}\right)}{4a^2\left[\wp_\eta\left(\frac{\tau-\tau_\eta}{a^2}\right) - B_\eta\right]^2}. \tag{78}$$

4 ANALYSIS OF THE RESULTS

In the previous sections, we computed the full exact solution of the three-dimensional E3BP. The evolution of the coordinates ξ, η and ϕ in fictitious time is given by equations (40), (53) and (67). The evolution in fictitious time of the momenta p_ξ and p_η is given by equations (75) and (76) (the third momentum, p_ϕ, is a constant of motion). The connection between the fictitious time τ and the real time t is given by equation (72). The equations are valid for all initial conditions and physical parameters of the three-dimensional system (that is, when p_ϕ is not zero).

The solutions for ξ, η, p_ξ and p_η are expressed solely in terms of the elliptic functions $\wp$ and $\wp'$. ξ and p_ξ are thus periodic functions of τ with period $2a^2\omega_\xi$, while η and p_η are periodic functions of τ with period $2a^2\omega_\eta$. In general, the two periods will be different.

[2] It must be noted how the right-hand sides of equations (63) and (64) have singularities when $\wp'(v)$ is zero. In this situation, alternative formulae need to be used, as detailed in Tannery & Molk (1893, Chapter CXII) and Gradshteĭn & Ryzhik (2007, section 5.141). We will not consider this special case here.

[3] We need to point out a potential problem in the numerical evaluation of the right-hand side of equation (63), related to the appearance of the multivalued complex logarithm. If one uses the principal value for ln, the right-hand side of equation (63) will be discontinuous in correspondence of the branch cuts. In appendix A2 of Biscani & Izzo (2014), we discuss in detail the problem, and we provide a solution based on the Fourier series expansion of $\ln\sigma(z)$.

The solutions for $\phi(\tau)$ and $t(\tau)$ involve also the Weierstrassian functions σ and ζ (see equations 63 and 64), which are *not* elliptic functions: they are *quasi-periodic* functions.[4] The fictitious time derivatives (57) and (58) of ϕ and t, however, involve only the function $\wp$ and they can be thus seen as sums of functions with two different periods, $2a^2\omega_\xi$ and $2a^2\omega_\eta$. Such functions are sometimes called *almost-periodic* functions (Besicovitch 1932).

In a way, the fictitious time τ can be considered as the E3BP analogue of the eccentric anomaly in the two-body problem. Kepler's equation for the elliptic two-body problem reads

$$t\left(E\right)=\frac{E-e\sin E}{n}, \tag{79}$$

where E is the eccentric anomaly, e the eccentricity of the orbit and n the (constant) mean motion. Clearly, Kepler's equation is structurally similar to (albeit much simpler than) equation (72): they are both transcendental equations featuring a combination of linear and periodic parts. Kepler's equation is a quasi-periodic function, so that

$$t\left(E+2\pi\right)=t\left(E\right)+\frac{2\pi}{n}. \tag{80}$$

In a similar fashion, $t(\tau)$ is the sum of two parts, one quasi-periodic with quasi-period $2a^2\omega_\xi$, the other quasi-periodic with quasi-period $2a^2\omega_\eta$. Following the nomenclature introduced earlier, we can then refer to $t(\tau)$ (and to $\phi(\tau)$ as well, since it is structurally identical) as an *almost quasi-periodic* function. In Section 4.2, we will examine periodicity and quasi-periodicity in the E3BP in more detail.

4.1 Boundedness and regions of motion

As we noted in the previous paragraph, the solution of the E3BP in terms of Weierstrassian functions is expressed as a set of unique formulae valid for all initial conditions and physical parameters of the system. That is, both bounded and unbounded orbits can be described by the same equations. Now, according to equations (8) and (9), the test particle can go to infinity only when ξ goes to infinity (by definition, the η coordinate is confined to the $[-1, 1]$ interval). The solution for $\xi(\tau)$, here reproduced for convenience,

$$\xi\left(\tau\right)=\xi_r+\frac{1}{4}\frac{f_\xi'\left(\xi_r\right)}{\wp_\xi\left(\frac{\tau-\tau_\xi}{a^2}\right)-\frac{1}{24}f_\xi''\left(\xi_r\right)}, \tag{81}$$

shows how the necessary and sufficient condition for the motion to be bounded is

$$\wp_{\xi,\min}>\frac{1}{24}f_\xi''\left(\xi_r\right), \tag{82}$$

where $\wp_{\xi,\min}$ is the minimum value assumed by $\wp_\xi$ in the real period $2\omega_\xi$. When this condition holds, the right-hand side of equation (81) has no poles and $\xi(\tau)$ is bounded. Vice versa, when the condition does not hold ξ will reach infinity in a finite amount of fictitious time. According to the theory of elliptic functions, within the real period and on the real axis

$$\wp_{\xi,\min}=\wp_\xi\left(\omega_\xi\right). \tag{85}$$

That is, the global minimum of $\wp$ on the real axis is in correspondence of the real half-period. In addition,

$$\wp_\xi\left(\omega_\xi\right)=e_i, \tag{86}$$

where e_i is one of the roots of the Weierstrass cubic (43). By using equations (86) and (85), we can thus rewrite the condition (84) as

$$e_i>\frac{1}{24}f_\xi''\left(\xi_r\right). \tag{87}$$

For unbounded orbits, we can compute the fictitious time at which ξ goes to infinity, τ_∞, using the condition

$$\wp_\xi\left(\frac{\tau_\infty-\tau_\xi}{a^2}\right)-\frac{1}{24}f_\xi''\left(\xi_r\right)=0, \tag{88}$$

that is,

$$\tau_\infty=\tau_\xi+a^2\wp^{-1}\left[\frac{1}{24}f_\xi''\left(\xi_r\right)\right]. \tag{89}$$

When the motion is unbounded τ_∞ is a real quantity, whereas when the motion is bounded τ_∞ becomes complex. With the definitions (73) and (60), we can rewrite equation (89) as

$$\tau_\infty=\tau_\xi+a^2\wp_\xi^{-1}\left(B_\xi\right). \tag{90}$$

We can then immediately verify how the substitution of τ_∞ for τ in equation (62) leads to the two denominators of the form

$$\wp_\xi\left(\frac{\tau-\tau_\xi}{a^2}\right)-B_\xi \tag{91}$$

on the right-hand side to go to zero. That is, for $\tau=\tau_\infty$ $\mathrm{d}t/\mathrm{d}\tau$ has a vertical asymptote, and the real time thus goes to infinity in a finite amount of fictitious time.

In contrast to $t(\tau)$, $\phi(\tau)$ has no asymptotes in fictitious time. For $\tau=\tau_\infty$, in unbounded orbits $\phi(\tau)$ assumes the finite value ϕ_∞ (which can be calculated via the substitution of τ_∞ for τ in equation 67). In the E3BP, ϕ_∞ plays the same role that the approach and departure angles play in hyperbolic trajectories in the two-body problem.

It should be noted that $\wp^{-1}$ is a multivalued function, and there are thus two possible values to choose from for τ_∞ within the fundamental parallelogram of $\wp$. This duality physically corresponds to the fact that unbounded orbits have two asymptotes, one inbound and one outbound. Correspondingly, there are two possible ϕ_∞ values, one at $t=-\infty$ and the other one at $t=\infty$. Fig. 5 illustrates graphically the evolution in fictitious time of the coordinates and of t in a representative unbounded trajectory.

It is worth stressing that, from a purely mathematical point of view, even in unbounded trajectories the evolution of ξ is still periodic. This periodicity is in fictitious time and it does not carry over to the evolution in real time because of the asymptotes in $t(\tau)$.

In bounded trajectories, by contrast, both ξ and η vary periodically within the finite ranges $[\xi_{\min}, \xi_{\max}]$ and $[\eta_{\min}, \eta_{\max}]$. Consequently, $t(\tau)$ has no asymptotes in bounded trajectories, and the periodicity of ξ and η in fictitious time translates to a periodicity in real time. Fig. 6 illustrates graphically the evolution in fictitious time of the coordinates and of t in a representative bounded trajectory.

[4] Here, we use the term 'quasi-periodic' in the following sense: a function f is quasi-periodic with quasi-period T if $f(z+T)=g(z,f(z))$. In the specific cases of σ and ζ, the following relations hold:

$$\sigma\left(z+T\right)=A\mathrm{e}^{zB}\sigma\left(z\right), \tag{83}$$

$$\zeta\left(z+T\right)=\zeta\left(z\right)+C, \tag{84}$$

where A, B and C are constants (Abramowitz & Stegun 1964, equations 18.2.19 and 18.2.20).

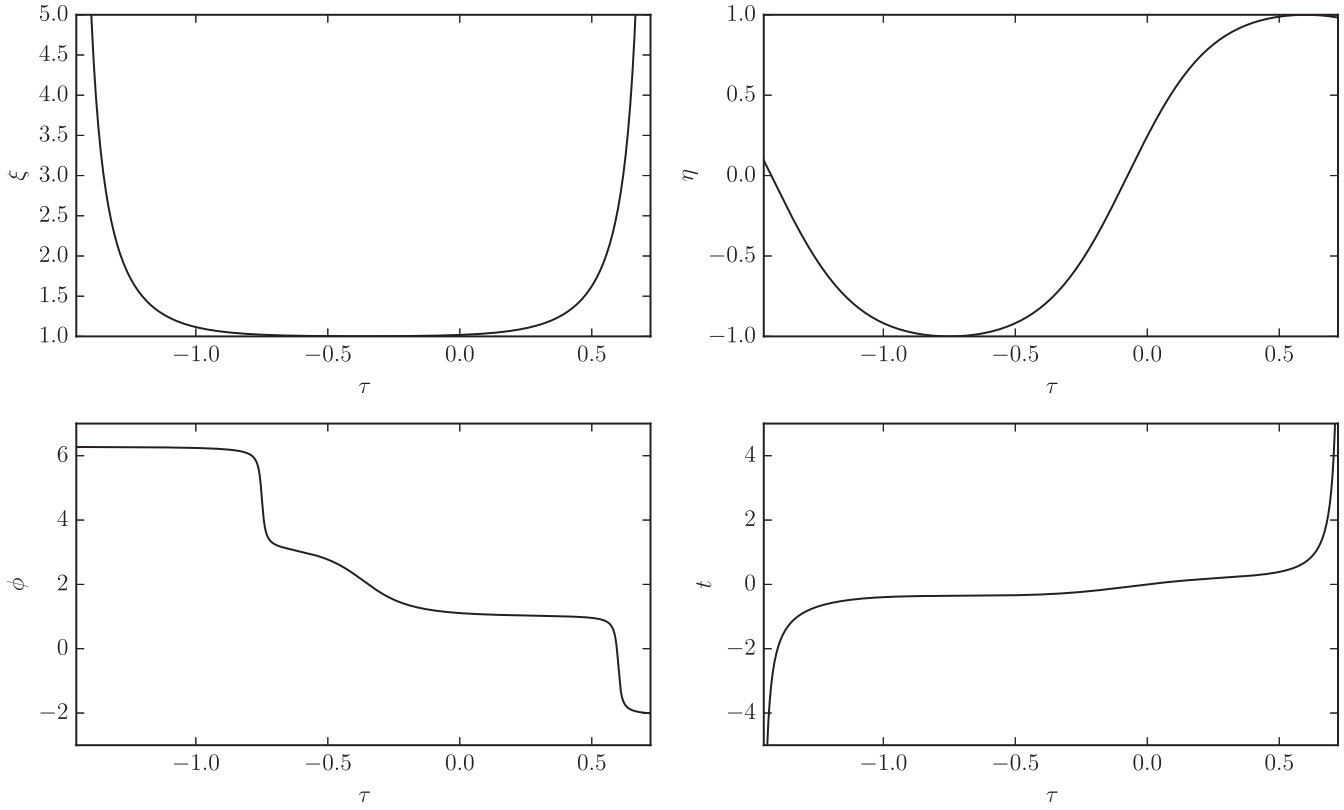

Figure 5. Evolution in fictitious time τ of the coordinates ξ, η and ϕ, and of the real time t in a representative unbounded orbit in the E3BP. $\xi(\tau)$ features two vertical asymptotes, reaching infinity in a finite amount of fictitious time. $t(\tau)$ also has two vertical asymptotes. $\eta(\tau)$ is bounded in the interval $[-1, 1]$ by its geometrical definition, and $\phi(\tau)$ assumes finite values when ξ and t go to infinity.

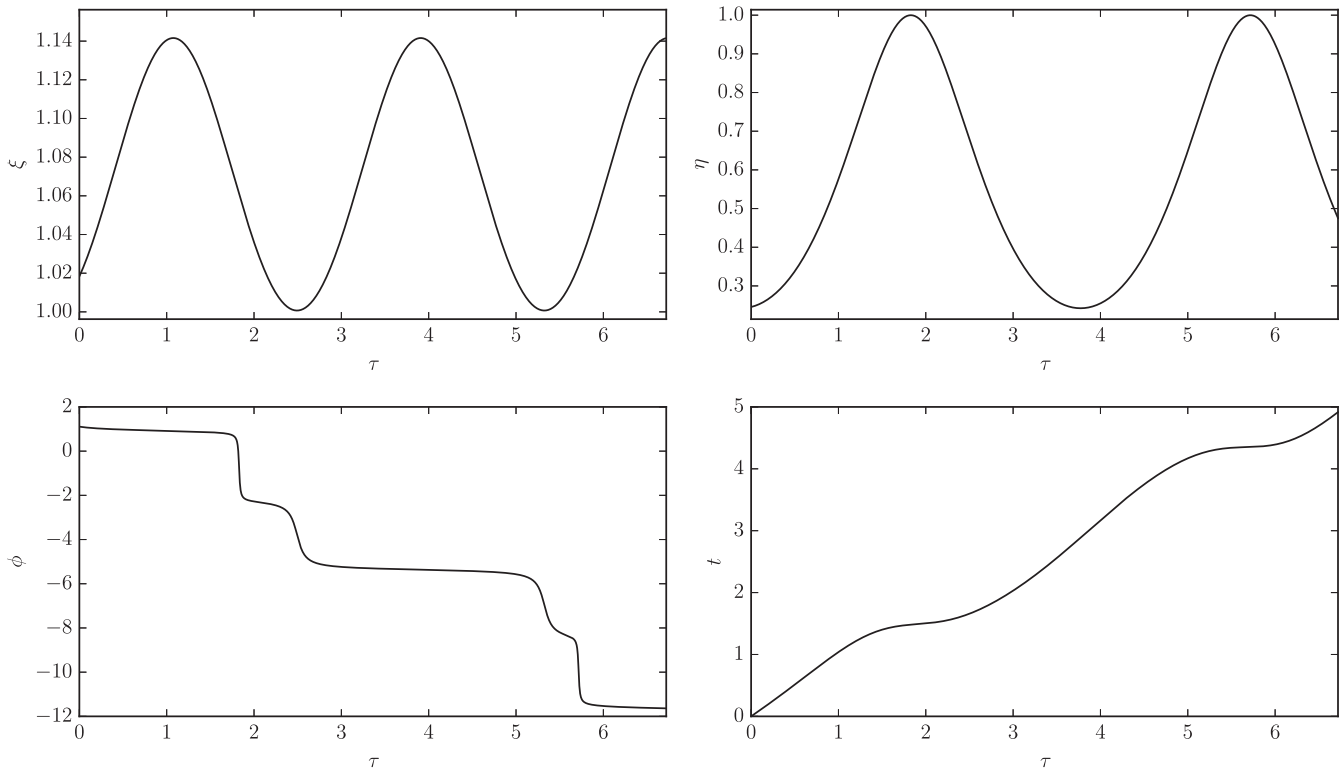

Figure 6. Evolution in fictitious time τ of the coordinates ξ, η and ϕ, and of the real time t in a representative bounded orbit in the E3BP. $\xi(\tau)$ and $\eta(\tau)$ are periodic functions with two different periods. $t(\tau)$ and $\phi(\tau)$ are almost quasi-periodic functions.

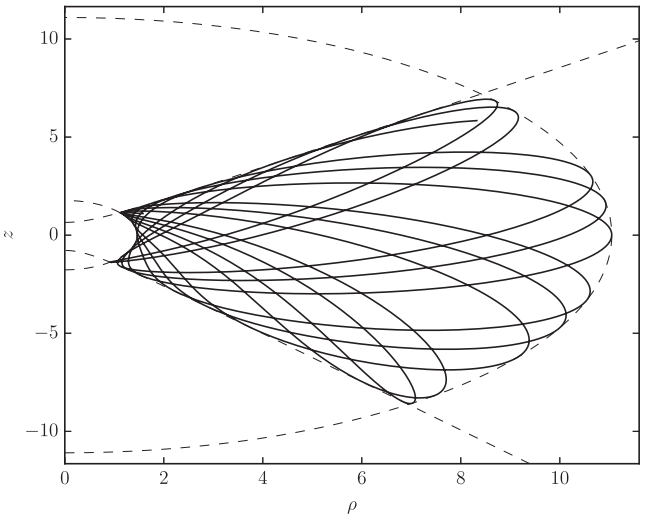

Figure 7. Regions of motion on the (ρ, z) plane in a representative bounded trajectory. The motion is confined within the two ellipses implicitly defined by $\xi(\rho, z) = \{\xi_{\min}, \xi_{\max}\}$ and within the two hyperbolic branches defined implicitly by $\eta(\rho, z) = \{\eta_{\min}, \eta_{\max}\}$. Both the ellipses and the hyperbolic branches are represented by the dashed lines. The solid line represents the actual trajectory of the test particle. The two centres of attraction are lying on the z-axis at $z = \pm 1$.

In Section 2, we introduced the elliptic–cylindrical coordinate system defined by equations (10) and (11):

$$\xi = \frac{\sqrt{\rho^2 + (z+a)^2} + \sqrt{\rho^2 + (z-a)^2}}{2a}, \tag{92}$$

$$\eta = \frac{\sqrt{\rho^2 + (z+a)^2} - \sqrt{\rho^2 + (z-a)^2}}{2a}. \tag{93}$$

For fixed values of ξ and η, these two equations define confocal ellipses and hyperbolic branches in the (ρ, z) plane. This means that, in bounded orbits, the motion of the test particle in the (ρ, z) plane is confined in the intersection of two geometric regions:

(i) an elliptic ring implicitly defined by the condition $\xi_{\min} \leq \xi \leq \xi_{\max}$,

(ii) a hyperbolic ring implicitly defined by the condition $\eta_{\min} \leq \eta \leq \eta_{\max}$.

The regions of motion in a representative bounded case are illustrated in Fig. 7.

We can explicitly compute the fictitious time at which ξ and η assume their minimum and maximum values. According to the theory of elliptic functions, $\wp_\xi$ has a global finite minimum on the real axis in correspondence of the real half-period ω_ξ (and, analogously, $\wp_\eta$ has a global minimum at ω_η). The global maximum for $\wp_\xi$ on the real axis is at $2k\omega_\xi$ ($k \in \mathbb{Z}$), where the value of the function is $+\infty$. Consequently:

$$\xi_{\min} = \xi\left(\tau_\xi\right), \quad \xi_{\max} = \xi\left(a^2\omega_\xi + \tau_\xi\right), \tag{94}$$

$$\eta_{\min} = \eta\left(\tau_\eta\right), \quad \eta_{\max} = \eta\left(a^2\omega_\eta + \tau_\eta\right). \tag{95}$$

4.2 Periodicity and quasi-periodicity

In the previous sections, we have mentioned how the evolution of ξ and η in fictitious time is periodic, with two periods that, in general, will be different. The periodicity in fictitious time of each coordinate translates to a periodicity in real time only for bounded orbits. By contrast, the evolution in fictitious time of the third coordinate ϕ and of the real time t derives from the integration of almost periodic functions, and it is thus almost quasi-periodic. We are now going to examine in more detail the behaviour of ϕ and t. We will focus on the study of $\phi(\tau)$, as $t(\tau)$ is structurally identical.

The derivative in fictitious time for $\phi(\tau)$, equation (57), can be seen as a linear combination of two periodic functions:

$$\frac{\mathrm{d}\phi}{\mathrm{d}\tau} = \frac{\mathrm{d}\phi_\xi(\tau)}{\mathrm{d}\tau} + \frac{\mathrm{d}\phi_\eta(\tau)}{\mathrm{d}\tau}, \tag{96}$$

where

$$\frac{\mathrm{d}\phi_\xi(\tau)}{\mathrm{d}\tau} = \frac{p_\phi}{a^2\left[\xi^2(\tau) - 1\right]}, \tag{97}$$

$$\frac{\mathrm{d}\phi_\eta(\tau)}{\mathrm{d}\tau} = \frac{p_\phi}{a^2\left[1 - \eta^2(\tau)\right]}. \tag{98}$$

The sign of $\mathrm{d}\phi/\mathrm{d}\tau$ is either always positive or always negative, depending on the sign of the constant p_ϕ, and thus $\phi(\tau)$ is a monotonic function. $\phi_\xi(\tau)$ is given by the terms in equation (67) related to ξ, and similarly $\phi_\eta(\tau)$ is given by the terms related to η, so that equation (67) can be written as

$$\phi(\tau) = \phi_0 + \phi_\xi(\tau) + \phi_\eta(\tau). \tag{99}$$

Since their derivatives are periodic functions with periods $2\omega_\xi$ and $2\omega_\eta$, $\phi_\xi(\tau)$ and $\phi_\eta(\tau)$ are arithmetic quasi-periodic functions with quasi-periods $2\omega_\xi$ and $2\omega_\eta$. That is, for any $\tau \in \mathbb{R}$,

$$\frac{\phi_\xi\left(\tau + 2\omega_\xi\right) - \phi_\xi(\tau)}{2\omega_\xi} = \Phi_\xi, \tag{100}$$

$$\frac{\phi_\eta\left(\tau + 2\omega_\eta\right) - \phi_\eta(\tau)}{2\omega_\eta} = \Phi_\eta, \tag{101}$$

where Φ_ξ and Φ_η are constants representing the average rate of change of $\phi_\xi(\tau)$ and $\phi_\eta(\tau)$. It follows then that the average rate of change of $\phi(\tau)$ is simply

$$\Phi_\xi + \Phi_\eta. \tag{102}$$

That is, $\phi(\tau)$ will oscillate almost periodically around a line parallel to the line

$$\left(\Phi_\xi + \Phi_\eta\right)\tau. \tag{103}$$

The situation is illustrated in Fig. 8.

The ratio between the periods of ξ and η, ω_ξ/ω_η, is in general a real value. If

$$\frac{\omega_\xi}{\omega_\eta} = \frac{n}{m}, \tag{104}$$

where n and m are two coprime positive integers, then ξ and η will share the same finite period $T = 2m\omega_\xi = 2n\omega_\eta$:

$$\xi(\tau) = \xi\left(\tau + 2m\omega_\xi\right) = \xi(\tau + T), \tag{105}$$

$$\eta(\tau) = \eta\left(\tau + 2n\omega_\eta\right) = \eta(\tau + T). \tag{106}$$

We refer to this case as an *isochronous* configuration. In an isochronous configuration, $\mathrm{d}\phi/\mathrm{d}\tau$ and $\mathrm{d}t/\mathrm{d}\tau$ become periodic functions of period T. $\phi(\tau)$ and $t(\tau)$ are integrals of periodic functions, and thus they are arithmetic quasi-periodic functions:

$$\phi(\tau + T) = \phi(\tau) + \phi_T, \tag{107}$$

$$t(\tau + T) = t(\tau) + t_T, \tag{108}$$

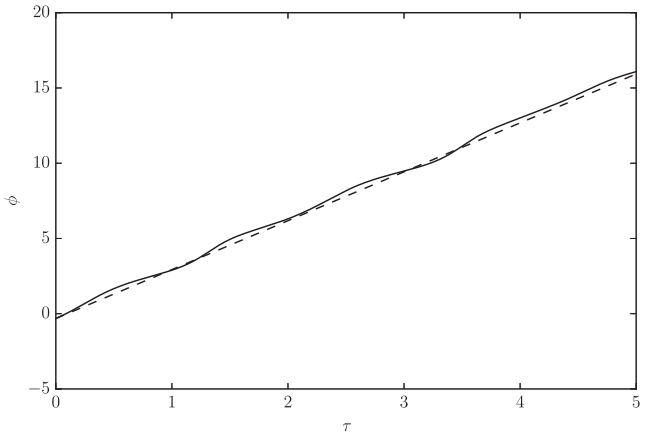

Figure 8. Evolution in fictitious time τ of the ϕ coordinate in a representative bounded trajectory in the E3BP. The solid line represents the actual evolution of the ϕ coordinate, while the dashed line represents the average rate of change of ϕ in fictitious time, which amounts to $\Phi_\xi + \Phi_\eta$ (see equation 103). ϕ is an almost quasi-periodic function of τ.

where ϕ_T and t_T are two constants depending only on the initial conditions and physical parameters of the system. From a geometric point of view, an isochronous configuration generates a quasi-periodic three-dimensional trajectory. That is, after a quasi-period T, the coordinates ξ and η and the momenta p_ξ and p_η will assume again their original values, while the coordinate ϕ will be augmented by ϕ_T.

It is possible to look for isochronous configurations by setting up a numerical search. After fixing two coprime positive integers n and m and the physical parameters of the system, the goal will be to find a set of initial conditions that minimises the quantity

$$\left| m\omega_\xi - n\omega_\eta \right|. \tag{109}$$

Such a search can be performed with standard minimization algorithms. In this case, we used the SLSQP algorithm from Kraft (1994), as implemented in the SCIPY PYTHON library (Jones et al. 2001). Fig. 9 displays a representative quasi-periodic trajectory found by a numerical search.

As a next step, we can look for periodic orbits: if, in an isochronous configuration, the ϕ_T constant is commensurable with 2π, then the trajectory of the test particle in the three-dimensional space will be a closed curve. In other words, the search for periodic orbits can be cast as the minimization of the function

$$\left| m\omega_\xi - n\omega_\eta \right| + \left| \phi_T \% \frac{2\pi}{k} \right|, \tag{110}$$

where n, m and k are positive integers, n and m are coprime and $\%$ is the modulo operator. Fig. 10 displays a representative periodic trajectory found by a numerical search.

4.3 Equilibrium points

In the last section of our analysis, we will briefly examine the equilibrium points in the E3BP. It is clear from the form of the Lagrangian (1) that in Cartesian coordinates there is an equilibrium point lying on the z-axis, where the forces exerted by the two bodies are balanced. This is a 'real' equilibrium point, in the sense that the test particle will be at rest if placed in this point with a null initial velocity. This equilibrium point corresponds to the $L_{1,2,3}$ Lagrangian points in the circular restricted three-body problem.

In elliptic–cylindrical coordinates, we cannot properly characterize the equilibrium point on the z-axis as it lies in correspondence of a singularity of the coordinate system. On the other hand, in elliptic–cylindrical coordinates we have another set of equilibrium points characterized by constant ξ and/or η. These are not equilibrium points in which the particle is at rest:

(i) if only ξ is constant, then the motion is confined to a section of the surface of an ellipsoid of revolution,
(ii) if only η is constant, then the motion is confined to a section of the surface of a hyperboloid of revolution,
(iii) if both ξ and η are constant, the motion is confined to a circle resulting from the intersection of an ellipsoid and a hyperboloid of revolution.

The third case, in particular, corresponds to the following initial setup:

(i) the net force acting on the particle is parallel to the xy plane,
(ii) the velocity vector of the particle is also parallel to the xy plane,
(iii) the direction and the magnitude of the velocity vector are those of a Keplerian circular orbit with a virtual centre of attraction on the z-axis, whose mass is exerting a force equal to the net force acting on the particle.

In other words, this case corresponds to a circular orbit parallel to the xy plane along which the z components of the forces from the two centres of attraction cancel each other, leaving a net force directed towards the z-axis. We refer to this particular setup as a *displaced circular orbit*.[5]

From the point of view of our solution to the E3BP, a displaced circular orbit is characterized by the solutions for ξ and η collapsing to constant functions. According to equations (40) and (53), this can happen only when

$$f'_\xi(\xi_r) = 0, \tag{111}$$

$$f'_\eta(\eta_r) = 0. \tag{112}$$

From the physical point of view, the balance of the z components of the two forces acting on the test particle leads to the following relation between ρ and z:

$$\rho = \sqrt{\frac{(a+z)^2\left[\mu_1(a-z)\right]^{2/3} - (a-z)^2\left[\mu_2(a+z)\right]^{2/3}}{\left[\mu_1(a-z)\right]^{2/3} - \left[\mu_2(a+z)\right]^{2/3}}}. \tag{113}$$

Given a pair of coordinates (ρ_d, z_d) satisfying equation (113), we can then compute the magnitude of the total net force acting on the test particle (parallel to the xy plane and directed towards the z-axis) as

$$F_d = \frac{\mu_1\rho_d}{\left[\rho_d^2 + (z_d - a)^2\right]^{2/3}} + \frac{\mu_2\rho_d}{\left[\rho_d^2 + (z_d + a)^2\right]^{2/3}}, \tag{114}$$

F_d corresponds to the force exerted by a virtual centre of attraction, lying at the coordinates $(0, z_d)$ in the (ρ, z) plane, whose gravitational parameter is

$$\mu_d = \rho_d^2 F_d. \tag{115}$$

[5] Displaced circular orbits are also present in the Stark problem, which is a limiting case of the gravitational E3BP (Namouni & Guzzo 2007; Lantoine & Russell 2011; Biscani & Izzo 2014).

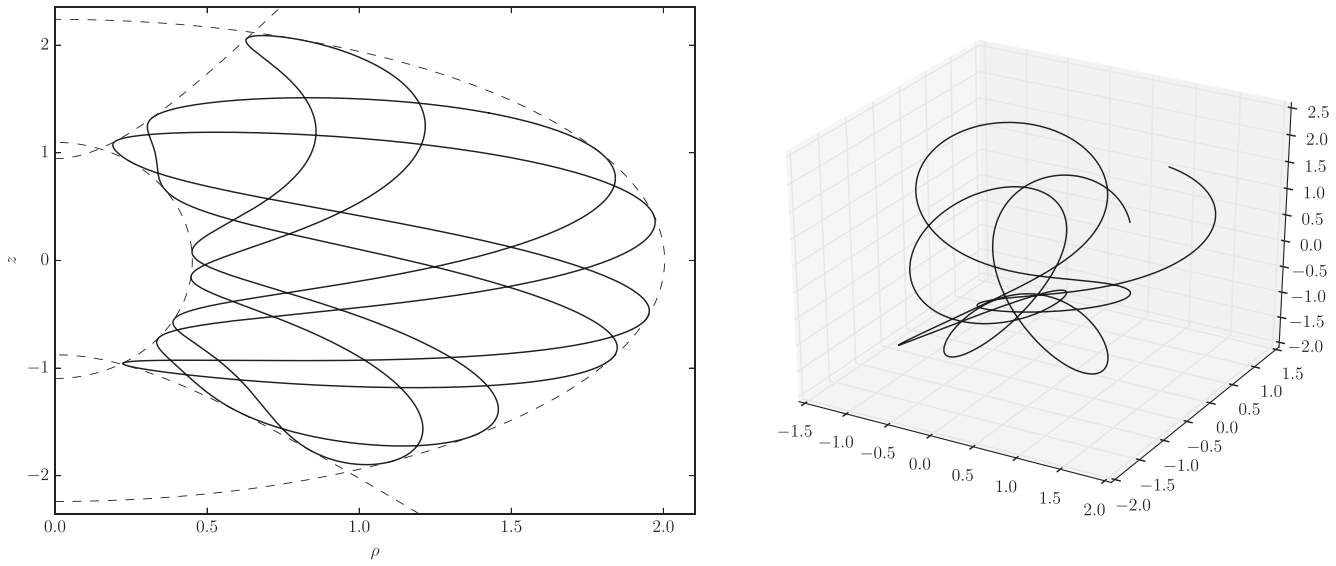

Figure 9. Graphical depiction of a representative quasi-periodic orbit in the E3BP over a single quasi-period. In this specific case, the periods of ξ and η are in a ratio of 3/7 with an accuracy of 10^{-14}. The left-hand panel displays the trajectory in the (ρ, z) plane (solid line), together with the boundaries of the region of motion (dashed lines). The right-hand panel displays the trajectory in the three-dimensional space. In quasi-periodic orbits, the trajectory in the (ρ, z) plane is a closed figure similar to a Lissajous curve (the difference being that here the periodic functions defining the figure are elliptic functions, rather than circular functions). In the three-dimensional space the trajectory is not closed: after one quasi-period ξ and η will assume again the original values, while ϕ will be augmented by a constant quantity.

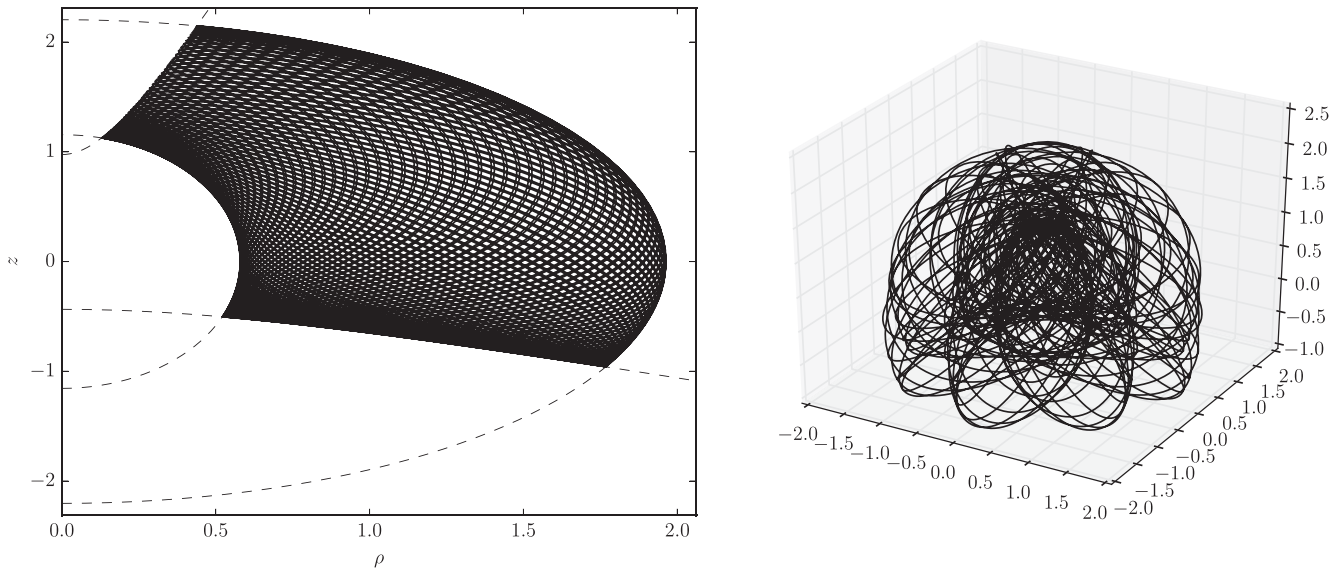

Figure 10. Graphical depiction of a representative periodic orbit in the E3BP over a single period. In this specific case, the periods of ξ and η are in a ratio of 91/99 with an accuracy of 10^{-13} and $\frac{\phi_T}{2\pi} = 96$ with an accuracy of 10^{-11}. The left-hand panel displays the trajectory in the (ρ, z) plane (solid line), together with the boundaries of the region of motion (dashed lines). The right-hand panel displays the trajectory in the three-dimensional space. Analogously to a quasi-periodic orbit, the trajectory in the (ρ, z) plane is a closed elliptic Lissajous figure. Unlike in the quasi-periodic case, the three-dimensional trajectory is also a closed figure. For this orbit, $a = 1$, $\mu_1 = 1$, $\mu_2 = .05$, the initial Cartesian position vector is (1.207 937 596 667 36, −0.493 320 558 636 725, 1.197 606 785 945 65), and the initial Cartesian velocity vector is (−0.498 435 147 674 914, 0.548 228 167 205 306, 0.496 626 916 283 632). The period is 405.074 289 498 234.

We can now use the well-known relation between gravitational parameter and orbital radius for circular Keplerian orbits to compute the velocity along a circular displaced orbit as

$$v_d = \sqrt{\frac{\mu_d}{\rho_d}}. \tag{116}$$

Figs 11 and 12 depict two representative slightly perturbed displaced circular orbits.

5 CONCLUSIONS AND FUTURE WORK

In this paper, we have presented for the first time a complete, closed-form solution to the three-dimensional problem of two fixed centres.

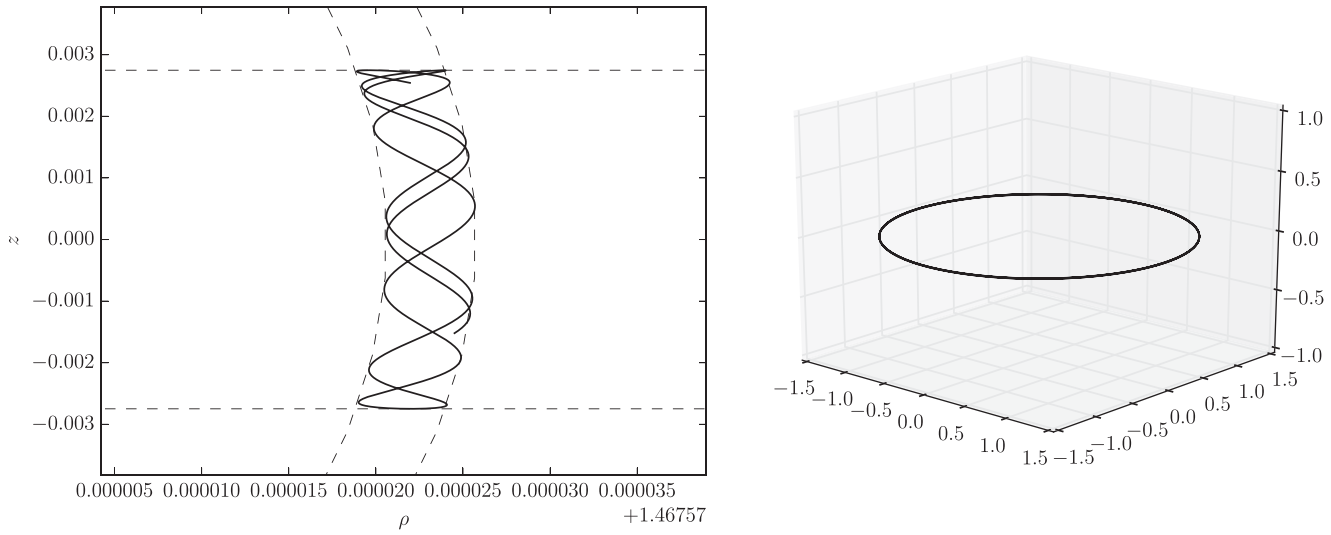

Figure 11. Graphical depiction of a slightly perturbed displaced circular orbit in the E3BP near the *xy* plane. The initial conditions have been chosen close to the setup described by equations (113) and (116). The left-hand panel displays the trajectory in the (ρ, z) plane (solid line), together with the boundaries of the region of motion (dashed lines). The right-hand panel displays the trajectory in the three-dimensional space.

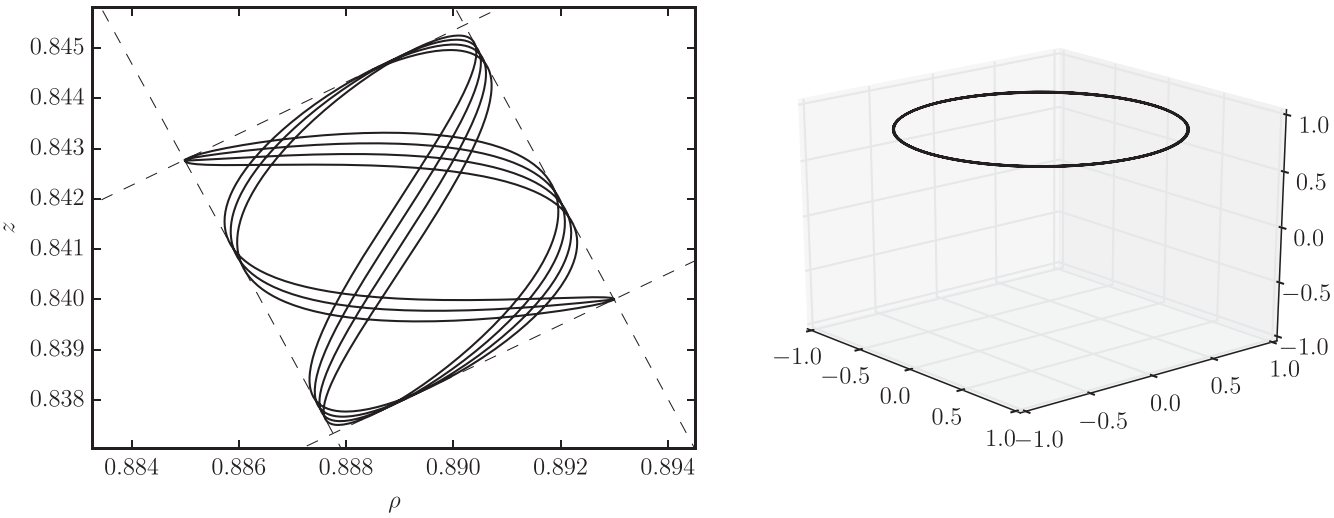

Figure 12. Graphical depiction of a slightly perturbed displaced circular orbit in the E3BP far from the *xy* plane. The initial conditions have been chosen close to the setup described by equations (113) and (116). The left-hand panel displays the trajectory in the (ρ, z) plane (solid line), together with the boundaries of the region of motion (dashed lines). The right-hand panel displays the trajectory in the three-dimensional space.

Our solution is based on the theory of Weierstrass elliptic and related functions, and it is expressed via unique formulae valid for any set of initial conditions and physical parameters of the system. Remarkably, our solution is strikingly similar to (albeit more complicated than) the solution of the two-body problem: the real time is substituted by a fictitious time, analogue to the mean anomaly in Kepler's problem, and the connection between real and fictitious time is established by an equation structurally similar to Kepler's equation.

The compact form of our solution allows us to investigate the properties of the dynamical system. In particular, we have formulated analytical criteria for quasi-periodic and periodic motion, and we have identified, via a simple numerical search, a few concrete representative quasi-periodic and periodic orbits. We have also discussed the dichotomy between bounded and unbounded orbits, the topology of the regions of motion, and we have identified displaced circular orbits as equilibrium points in elliptic–cylindrical coordinates.

In future papers, we will focus on the physical and astronomical applications of the results presented here. Of particular interest are the application of our solution to the Vinti potential and the interpretation of the E3BP as a limiting case of the circular restricted three-body problem.

REFERENCES

Abramowitz M., Stegun I. A., 1964, Handbook of Mathematical Functions with Formulas, Graphs, and Mathematical Tables. Dover Press, New York

Akhiezer N. I., 1990, Elements of the Theory of Elliptic Functions. Am. Math. Soc., Providence, RI

Aksenov Y. P., Grebenikov Y. A., Demin V. G., 1962, Planet. Space Sci., 9, 491
Aksenov Y. P., Grebenikov Y. A., Demin V. G., 1963, SvA, 7, 276
Alfriend K. T., Dasenbrock R., Pickard H., Deprit A., 1977, Celest. Mech., 16, 441
Arnold V. I., 1989, Mathematical Methods of Classical Mechanics, 2nd edn. Springer-Verlag, Berlin
Besicovitch A. S., 1932, Almost Periodic Functions. Cambridge Univ. Press, Cambridge
Biscani F., Izzo D., 2014, MNRAS, 439, 810
Carinena J. F., Ibort L. A., Lacomba E. A., 1988, Celest. Mech., 42, 201
Charlier C. V. L., 1902, Die Mechanik des Himmels. Leipzig, Veit
Coelho F. S., Herdeiro C. A. R., 2009, Phys. Rev. D, 80, 104036
Cordani B., 2003, The Kepler Problem: Group Theoretical Aspects, Regularization and Quantization, with Application to the Study of Perturbations. Birkhuser Verlag, Basel, Boston
Darboux G., 1901, Arch. Néerlandaises Sci. Exactes Naturelles, 6, 371
Demin V. G., 1961, SvA, 4, 1005
Deprit A., 1962, Bull. Soc. Math. Belg., 14, 12
Gradshteĭn I. S., Ryzhik I. M., 2007, Table of Integrals, Series, and Products. Academic Press, New York
Greenhill G., 1959, The Applications of Elliptic Functions. Dover Press, New York
Halphen G. H., 1886, Traité des fonctions elliptiques et de leurs applications. Vol. 1, Gauthier-Villars, Paris
Hiltebeitel A. M., 1911, Am. J. Math., 33, 337
Jones E. et al., 2001, SciPy: Open Source Scientific Tools for Python
Kraft D., 1994, ACM Trans. Math. Softw., 20, 262
Lantoine G., Russell R., 2011, Celest. Mech. Dyn. Astron., 109, 333
Namouni F., Guzzo M., 2007, Celest. Mech. Dyn. Astron., 99, 31
Ó'Mathúna D., 2008, Integrable Systems in Celestial Mechanics. Springer-Verlag, Berlin
Pauli W., 1922, Ann. Phys., Lpz., 373, 177
Saha P., 2009, MNRAS, 400, 228
Siegel C. L., Moser J. K., 1971, Lectures on Celestial Mechanics. Springer-Verlag, Berlin
Sundman K. F., 1912, Acta Math., 36, 105
Tannery J., Molk J., 1893, Éléments de la Theorié des Fonctions Elliptiques, Vol. 4. Gauthier Villars Et Fils Imprimeurs, Paris
Varvoglis H., Vozikis C., Wodnar K., 2004, Celest. Mech. Dyn. Astron., 89, 343
Vinti J. P., 1959, Mathematics and Mathematical Physics. J. Res. Natl. Bur. Stand. B, 62, 105
Waalkens H., Dullin H. R., Richter P. H., 2004, Nonlinear Phenomena. Physica D, 196, 265
Whittaker E. T., Watson G. N., 1927, A Course of Modern Analysis, 4th edn. Cambridge Univ. Press, Cambridge

APPENDIX A: SOLUTION ALGORITHM

In this section, we are going to detail the steps of a possible implementation of our solution to the three-dimensional E3BP, starting from initial conditions in Cartesian coordinates. The algorithm outlined below requires the availability of implementations of the Weierstrassian functions $\wp$, $\wp'$, $\wp^{-1}$, ζ and σ, and of a few related ancillary functions (e.g. for the conversion of the invariants g_2 and g_3 to the periods).

The algorithm is given as follows.

(i) Transform the initial Cartesian coordinates into initial elliptic–cylindrical coordinates ξ, η and z, and compute the initial Hamiltonian momenta p_ξ, p_η and p_ϕ. The formulae for these transformations are available in Section 2.

(ii) Compute the constants of motion h, h_ξ and h_η, through the substitution of the initial Hamiltonian coordinates and momenta into equations (23), (30) and (31).

(iii) Compute the values of the invariants g_2 and g_3 for both $\wp_\xi$ and $\wp_\eta$, using equations (41), (42), (54) and (55). The periods of $\wp_\xi$ and $\wp_\eta$ can be determined from the invariants using known formulae (see e.g. Abramowitz & Stegun 1964, Chapter 18).

(iv) Determine the roots ξ_r and η_r of the polynomials (34) and (51). Since these are quartic polynomials, there are four possible values for each root. We can immediately discard complex roots and those roots whose values are outside the domains of interest for the variables (i.e. $(1, +\infty)$ for ξ and $(-1, 1)$ for η). Note that complex roots and roots outside the domain of physical interest can still be used for the computation of the solution, but they lead to complex-valued times of pericentre passage and they have no immediate physical interpretation.

(v) Using the surviving values for ξ_r and η_r, compute the times of pericentre passage τ_ξ and τ_η via equations (48) and (56). As explained at the very end of Section 3.1, the calculation of τ_ξ and τ_η via $\wp^{-1}$ produces a pair of values for each ξ_r and η_r. We can immediately discard the values of ξ_r and η_r which result in complex τ_ξ and τ_η, for they correspond to unreachable roots.

(vi) At this point either one (for unbounded motion) or two (for bounded motion) values for ξ_r and η_r remain, both real. We select the smaller values for ξ_r and η_r (as we are interested in the times of *pericentre* passage), and we compute the corresponding pairs of values for τ_ξ and τ_η via equations (48) and (56). These pairs of values will all be real and positive. We select the smaller values for both times of pericentre passage and we check the sign of the initial values for $\mathrm{d}\xi/\mathrm{d}\tau$ and $\mathrm{d}\eta/\mathrm{d}\tau$: if they are positive, we negate the corresponding time of pericentre passage (as the pericentre was reached *before* $\tau = 0$), otherwise we can leave them as they are (as the pericentre will be reached *after* $\tau = 0$).

(vii) After having determined ξ_r, τ_ξ, η_r and τ_η we have all the ingredients to implement the solutions for the three coordinates, their conjugate momenta and the time equation (equations 40, 53, 67, 72, 75 and 76).

The procedure outlined above assumes the following conventions:

(i) the period pairs for $\wp_\xi$ and $\wp_\eta$ are chosen as explained in Section 3.1: the first period is always real and positive, the second one is always complex with positive imaginary part;

(ii) the $\wp^{-1}$ function returns a pair of values within the fundamental parallelogram defined by the periods pair.

APPENDIX B: CODE AVAILABILITY

We have implemented our solution to the E3BP in an open-source PYTHON module which is freely available for download here: https://github.com/bluescarni/e3bp.

The module depends on the `w_elliptic` PYTHON/C++ library, which provides an implementation of the Weierstrassian functions. The code is available here: https://github.com/bluescarni/w_elliptic.

All the numerical computations and all the graphs presented in the paper have been implemented with and produced by these two software modules.

This paper has been typeset from a TEX/LATEX file prepared by the author.